Journal of Inorganic and Organometallic Polymers and Materials (2021) 31:2615–2626
https://doi.org/10.1007/s10904-021-01914-5

Nickel and sulfur codoped TiO_2 nanoparticles for efficient visible light photocatalytic activity

Mehala Kunnamareddy[1] · **Ranjith Rajendran**[2] · **Megala Sivagnanam**[2] · **Ramesh Rajendran**[2] · **Barathi Diravidamani**[1]

Received: 21 October 2020 / Accepted: 20 January 2021 / Published online: 1 February 2021

Abstract

In this work, Nickel (Ni) and sulfur (S) codoped TiO_2 nanoparticles were prepared by a sol-gel technique. The as-prepared catalyst was characterized using X-ray diffraction (XRD), Fourier transforms infrared spectroscopy (FTIR), FT-Raman spectroscopy, scanning electron microscopy (SEM), energy dispersive spectrometer (EDS), transmission electron microscopy (TEM), UV-Vis diffuse reflectance spectra (DRS) for investigating crystal structure, crystal phase, particle size and bandgap energy of these samples. The photocatalytic performances of all the prepared catalysts have been investigated for the degradation of methylene blue (MB) under visible light irradiation. It was noticed that Ni-S codoped TiO_2(Ni-S/TiO_2) nanoparticles exhibited much higher photocatalytic activity compared with pure, Ni and S doped TiO_2 due to higher visible light absorption and probable decrease in the recombination of photo-generated charges. It was decided that the great visible light absorption was created for codoped TiO_2 by the formation of impurity energy states near both the edges of the collection, which works as trapping sites for both the photogenerated charges to decrease the recombination process.

Keywords Photocatalyst · Methylene Blue · Optical properties · Codoped TiO_2

1 Introduction

The continuous industrial development and the population growth level have directed extensive worries on environmental policies. Especially, water pollution has become one of the dangerous environmental issues. Therefore, the removal of organic contamination from wastewater is of great significance to environmental safety. Nowadays, various methods have been developed for removing dyes from aqueous media, such as physical adsorption, biodegradation, chemical oxidation, and photocatalytic degradation. Among them, the semiconductor-based photocatalysis process is one of the extensively adopted techniques for removing the dyes of organic pollutants and pharmaceutical waste from the water bodies. Because the semiconductor-based materials have a suitable band structure with the illuminated appropriate light source, the electrons, and holes are generated which can potentially produce hydroxyl radicals ($^{\cdot}OH$) and superoxide radicals ($^{-\cdot}O_2$) through various light-driven chemical reactions. Thus the widely-studied semiconductor photocatalysts are CeO_2, ZnO, TiO_2, CdS, Ta_3N_5, $PbWO_3$, NiO, and $BiFeO_3$ are proved to be an effective photocatalyst [1–9].

Among the several semiconducting photocatalysis, TiO_2 has been considered a promising product in the photocatalytic process due to its high photocatalytic activity, chemical stability, non-toxicity, relatively inexpensive, and showing substantial UV light absorption. The photocatalytic efficiency towards the degradation of various model-contaminants, such as formic acid, phenol, oxalic acid, and methyl orange [10–14]. This worked on the principle that a generation of electron-hole pairs occurred when the light fell on the TiO_2 surface. The photogenerated electron-hole pairs reacted with water and oxygen adsorbed on the surface of the sample. However, TiO_2 could be excited only under UV irradiation due to its large bandgap and there was also a high rate of electron-hole recombination, which decreases its photocatalytic activity of TiO_2 [15, 16]. Therefore, the most important and challenging issue is to develop efficient visible light-responsive photocatalysts by the modification of TiO_2. To overcome this challenge, the transition metal-doped TiO_2 was an effective technique for enhancing TiO_2

✉ Barathi Diravidamani
barathinkrgacphysics@gmail.com

[1] Department of Physics, N.K.R. Govt. Arts College for Women, Namakkal, Tamilnadu 637 001, India

[2] Department of Physics, Periyar University, Salem, Tamilnadu 636 011, India

absorption into the visible region and improving its photocatalytic operation [17].

Over the past decades, the doped of various transition metals has been widely studied to improve the photocatalytic performance of TiO_2, like Mo, Fe, Cr, Co, Mn, Ni, and Cu into TiO_2 to change its bandgap and photocatalytic activity [18, 19]. Another approach to sensitize TiO_2 in visible light is doping with non-metal elements such as nitrogen, carbon, sulfur, and iodine [20–29]. Transition metal ions and non-metallic elements doping can increase the quantum efficiency of TiO_2 and create surface defects to decrease the photogenerated electron-hole recombination rate. However, these may also act as recombination sites for the photoinduced charge carriers, lowering the quantum efficiency. [30, 31]. Recently, the codoping has been discovered to be a unique method for enhancing TiO_2 photocatalytic activity. Codoping has been shown to increase the specific area of the surface, enhance the visible light absorption, and prolong the lifespan of photogenerated charging carriers. Based on data published the use of metal-nonmetal co-doping could significantly improve the photocatalytic activity [32, 33].

In the present work, we employed the approach of codoping of Ni as a metal dopant and sulfur as a nonmetal dopant. It is well known that Ni ion is a more efficient dopant for TiO_2, as it can improve electrical and magnetic properties. The reason for this enhancement has been tentatively ascribed to the suppression of electron-hole pair recombination on the surface of the TiO_2 catalyst by low valence Ni^{2+} ions [34]. This upgraded activity was recognized as the enhanced separation of photo-generated electron-hole pairs due to the presence of Ni^{2+} ions in TiO_2 [35]. Sulfur was selected as a nonmetal dopant because it has long been investigated as an effective nonmetal dopant for the improvement of the visible light response of TiO_2. As for S doping, it was an exception for S^{2-} replacing O^{2-}, S^{4+}, or S^{6+} can too substitute for Ti^{4+} by cationic doping, which sources the visible light absorbance [36]. There were many techniques available to make the photocatalysts of pure and doped TiO_2. Sol-gel technique was one of the most common methods of synthesizing TiO_2-based photocatalysts because of its simplicity, low-temperature requirements, low cost, and a high potential for surface properties and controlling oxide substance [37, 38].

2 Materials and Methods

2.1 Materials

Titanium tetra isopropoxide ($Ti[OCH(CH_3)_2]_4$) (TTIP, Sigma-Aldrich), nickel nitrate ($Ni(NO_3)_2$) (Sigma-Aldrich), thiourea (NH_2CSH_2N) (Merck)isopropyl alcohol (C_3H_8O) (Sigma-Aldrich),and ethanol absolute (C_2H_6O) (99% Merck). All reagents were used without further purification as they were received.

2.2 Methods

The Ni and S codoped TiO_2 nanoparticles were prepared by a sol-gel method. In a typical procedure, 2.8 ml of TTIP was dissolved in 10 mL of isopropyl alcohol under constant stirring for about 30 min. As a codopant source, 0.07269 of nickel nitrate that was sufficiently added in 10 ml of deionized water and 0.01903 g of thiourea with 10 ml of deionized water were added dropwise into the above solution. The obtained homogeneous solution was stirred constantly for 5 h. Finally, the resulting precipitates were washed numerous times with deionized water and ethanol, centrifuged to remove soluble impurities. The washed samples were dried in air at 100 °C for 6 h and, finally, calcined at 450 °C for 4 h to obtain Ni/S-TiO_2 NPs. For comparison, the synthesis of pure TiO_2 nanoparticles was the same as the above-mentioned procedure, except for the absence of hydrofluoric acid and sodium tungsten. The synthesis of Ni-TiO_2 nanoparticles was the same as the above-mentioned procedure, except for the absence of thiourea. The synthesis of S-TiO_2 nanoparticles was the same as the above-mentioned procedure, except for the absence of nickel nitrate. The pure TiO_2also the same procedure except for the absence of nickel nitrate and thiourea [39].

2.3 Characterizations

Study of X-ray powder diffraction performed at room temperature using Rigaku Miniflex X-ray diffractometer device fitted with a Cu-tube to produce CuKα radiation ($\lambda = 1.5406$ Å). The incident beam operated at 40 kV and 30 mA in 2θ mode over the range of 20°-80° with a scanning rate of 5° min^{-1}. The prepared nanoparticles were recorded on FTIR and FT-Raman Spectrometer using a Model Brucker Tensor 27 and BrukerRFS27 spectrophotometer with a resolution of 2 cm^{-1} between 4000 and 400 cm^{-1} and 5000–50 cm^{-1} at KBr phase. To investigate the photocatalyst absorption spectra, the sample of UV-Vis diffuse reflectance spectra (DRS) was found using U-3010, a Hitachi system with $BaSO_4$ spectrophotometer at 200–800 nm wavelength. The synthesized sample of surface morphology and particle size was examined by scanning electron microscope (SEM) with model number JEOL JSM6390, fitted with energy dispersive X-ray analysis (EDX) to determine the elemental structures of nanoparticles. A transmission electron microscope (TEM) functioned at an accelerating voltage of 80 kV characterized the size and morphology of nanoparticles. The structure and crystalline nature were measured with a 200 kV powered High-Resolution Transmission electron microscope (HR-TEM) with an FEI Tecnai G2 F20 instrument. The prepared sample of photocatalytic activity has been measured in terms of methylene blue degradation. Use of the UV-Vis spectrophotometer (Ocean Optics PX-2) to monitor the level of Ni-S codoped TiO_2 degradation.

2.4 Electrochemical measurement

The Mott-Schottky plots were conducted by Bio-Logic SP-150 electrochemical workstation in 1 M KOH electrolyte solution with the three-electrode system. Fluorine doped tin oxide (FTO), Pt, and Ag/AgCl electrodes were used as working, counter, and reference electrodes respectively. The catalyst was coated on the working electrode by using a spin coating technique. A xenon lamp with a solar AM 1.5 illumination (100 $mW.cm^{-2}$) was used as a light source. The MS plots were generated in the dark for bias voltages from −1 V to 0 V.

2.5 Photocatalytic experiments

The photocatalytic activities of the prepared samples were estimated by the degradation of methylene blue (MB) under visible light irradiation. The source of light was a 500 W halogen lamp that could release visible light to penetrate the reactor. The distance between the sample and the lamp was 9 cm. The light intensity was 4.9 mW/m^2. In a characteristic procedure, 50 mg of photocatalysts were added into 100 ml of a 30 mg/L dye solution with constant magnetic stirring fitted with a water movement capacity. The reaction mixture was held in dark adsorption with stirred for 30 min before the photocatalytic reaction to achieve the organic dye adsorption equilibrium on the photocatalytic surface. The suspension was then continuously moved and exposed to the irradiation of visible light. 5 ml of the reaction solution was collected at regular intervals and centrifuged at 5000 rpm to extract the suspended photocatalyst on the solution. Using the collected sample, the UV-vis spectrometer was tested to determine the concentration of MB dye in the reaction solution and the concentration of MB at 660 nm was monitored.

3 Results and Discussion

3.1 XRD analysis

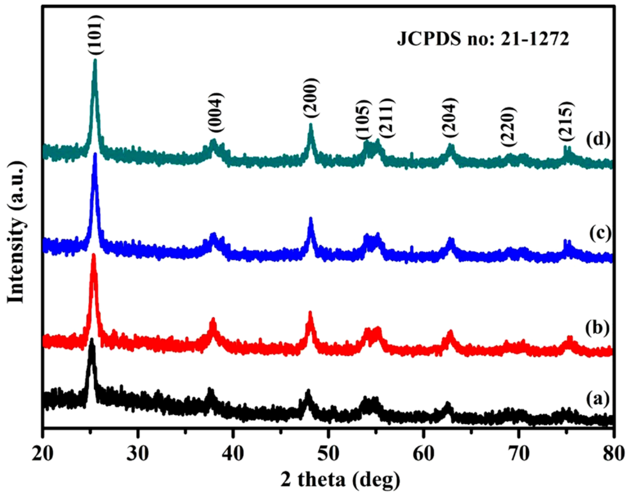

Fig. 1 Powder XRD forms of TiO_2 nanoparticles: (a) Pure TiO_2 (b) Ni/TiO_2 (c)S/TiO_2 (d) Ni-S/TiO_2

Figure 1 showed the X-ray diffraction patterns of the prepared pure, Ni-doped (Ni/TiO_2), S-doped (S/TiO_2), and Ni-S codoped TiO_2(Ni-S/TiO_2) nanoparticles. The diffraction peaks at 2θ values were at 25.1, 37.86, 48.8, 54.02, 55.26, 62.78, 68.88 and 75.38 respectively corresponding to (101), (004), (200), (105), (211), (204), (220) and (215) planes. Such peaks corresponded to the anatase phase of TiO_2 (JCPDS 21–1272) [40]. The same dopant in a replacement form could increase the level of oxygen vacancy and consequently promote the transformation of the phase, whereas the lattice constant could be strengthened in the interstitial form and thus inhibit the transformation of the phase. Generally, this principle extended to all dopants, while metal transition ions such as Fe, Ni, and Mn with variable valence display more mixed effects [41]. In the specific case of inhibition of phase transformation, Ni was needed to occupy the interstitial size in the synthesized samples. Usually, the occurrence of interstitial ions and the decrease in the anatase phase of interstitial particle interaction inhibited the transition. The crystallite size was estimated using the Debye-Scherrer formula [42].

$$D = k\lambda/\beta\cos\theta \tag{1}$$

where D is the crystallite size, λ is the wavelength, *k* is the shape factor and β is full width at the half maximum. The crystallite size of pure, Ni/TiO_2, S/$TiO_2$and Ni-S/TiO_2 calculated the sample values were 19, 13, 15, and 9 nm, respectively. Besides, the size of crystallite reduced with the rise in dopant concentration, which could be ascribed to peak expansion owing to defects in doped nanoparticles caused by dopant. Furthermore, no unique peak corresponding to Ni/NiO was noted, which could be due to the good dispersion of metal particles on TiO_2 or very low metal content [43].

3.2 Morphological Analysis

The detected scanning electron microscope (SEM) images of the as-prepared samples were shown in Fig. 2a-d. Figure 2(a) pure TiO_2 (b) Ni/TiO_2 (c) S/TiO_2nanoparticles were fairly uniform in size and with their agglomeration, a big amount

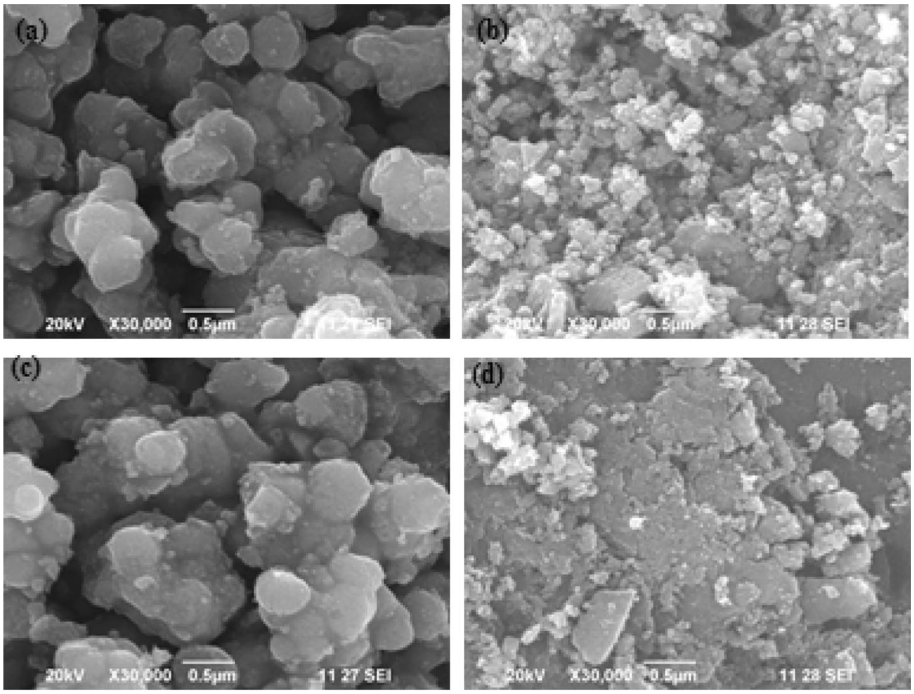

Fig. 2 SEM image of samples **a** pure TiO_2, **b** Ni/TiO_2, **c** S/TiO_2 and **d** Ni-S/TiO_2 nanoparticles

of pores were created. Figure 2 (d), displays the most of the particles were almost spherical with uniform size distribution [44]. Besides, the Ni and S have been highly dispersed in the surfaces of the TiO_2 lattices. To explore the further deep surface morphologies by transmission electron microscope (TEM) images of pure and Ni-S/TiO_2 samples shown in Fig. 3. The particle size of the pure sample has obtained the range from 15 to 18 nm (Fig. 3a) and at the same time, the codoped sample has obtained the range of 9 to 12 nm (Fig. 3b) which was in a good deal with that determined from XRD forms. The lattice-resolved HRTEM image Ni-S/TiO_2 (Fig. 3c) demonstrated, which specifies that the sample contains a fine crystallized lattice with the lattice spacing (d = 0.34 nm) corresponding to the (101) plane of TiO_2. Figure 3d displayed the corresponding SAED patterns of Ni-S codoped TiO_2 nanoparticles.

3.3 Elemental Analysis

The EDAX analysis of the Ni-S/TiO_2 nanoparticle was demonstrated in Fig. 4. It precisely displayed that the co-doped TiO_2 consists of Ti, Ni, O, and S. Each of the peaks was particular to an atom or resembles an element. The peak intensity denoted the concentration level of the element in the nanoparticles. Even though the low doping amount of nickel and sulfur, the observed peaks of Ni and S indicated that they were dispersed uniformly in the photocatalyst structure. The distinguished Ni-S/TiO_2 spectra explored the presence of Ti, O, Ni, and S elements with the atomic percentage 74.16, 24.39, 0.82, and 0.63%, the weight percentage were 48.72, 49.14, 1.02, and 1.12% respectively.

3.4 Fourier transform infrared spectroscopy

Figure 5 shown that all the samples were designed in the range of 4000–400 cm^{-1}. This figure cleared that to improve the visibility of the bands. Here the bands were corresponding to the expansion of O-H vibrations and bending vibrations of adsorbed water molecules between 1620 and 1635 and 3300–3450 cm^{-1} [45]. The band rate between 2800 and 3000 cm^{-1} and also 1300 and 1500 cm^{-1} indicated the presence in the nanoparticles of a small amount of organic material [46, 47]. The absorption was due to -C-H stretching vibration at 1396 cm^{-1} corresponding to the residual organic material contaminant on the surface from alkoxide precursor [48, 49]. It was possible to enlarge the width of the intermolecular or intramolecular bond. The band was about 500 cm^{-1} due to stretching Ti-O and Ti-O-Ti bond vibrations. Also, in this case of doped and codoped TiO_2 nanoparticles, the band shifted to lower wavenumber, hence these indicated that the sharp peaks would becomebroaden [50, 51].

3.5 Raman Spectra

Raman spectra of pure, Ni, Sand Ni-S/TiO_2 were depicted in Fig. 6. TiO_2 has six Raman active modes in the vibrational spectrum centered around 144 cm^{-1}, 197 cm^{-1}, 399 cm^{-1}, 513 cm^{-1}, 519 cm^{-1}, and 639 cm^{-1} corresponding to E_g,

Fig. 3 The TEM images of **a** pure TiO_2 and **b-d** Ni-S/TiO_2 nanoparticles

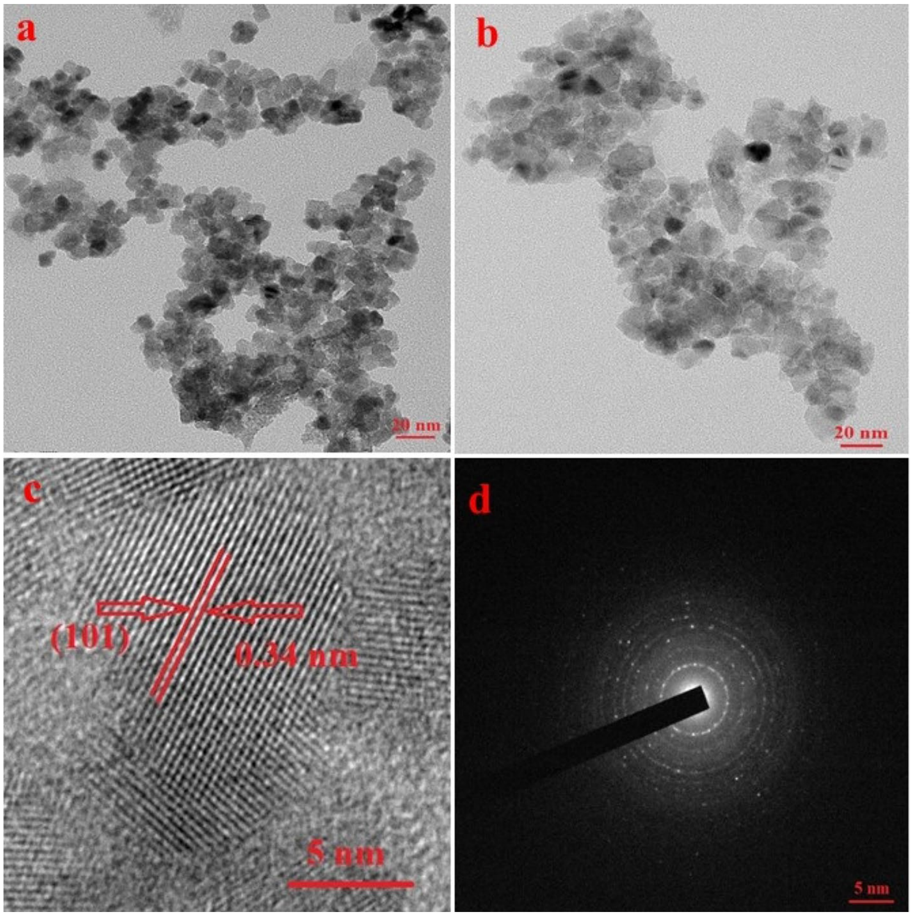

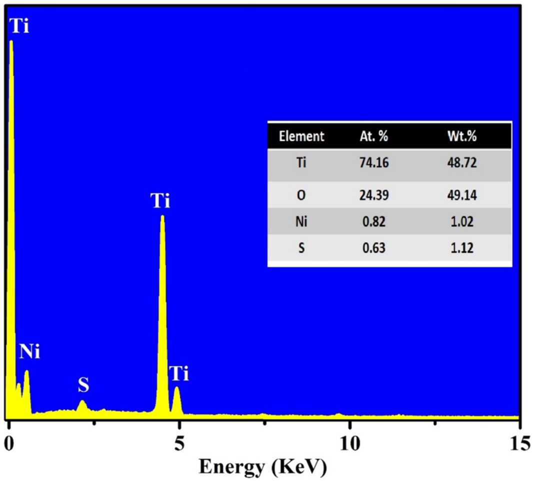

Element	At. %	Wt.%
Ti	74.16	48.72
O	24.39	49.14
Ni	0.82	1.02
S	0.63	1.12

Fig. 4 EDX spectrum of Ni-S/TiO_2 nanoparticle

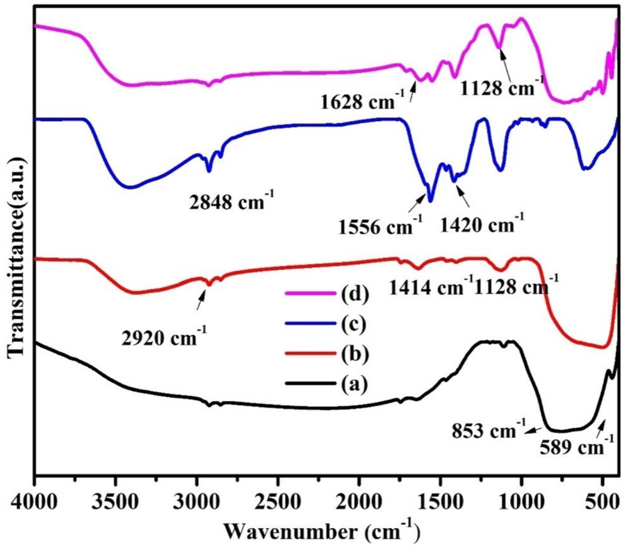

Fig. 5 FTIR spectra of (a) pure TiO_2 (b) Ni/TiO_2 (c) S/TiO_2 (d) Ni-S/TiO_2 nanoparticles

E_g, B_{1g}, A_{1g}, B_{1g} and E_g respectively [52]. In this study, the Raman spectra modes were noticed for pure TiO_2at 143 (E_g), 395 (B_{1g}), 516 ($A_{1g}+B_{1g}$), and 639 cm^{-1} (E_g) with slight widening, as compared with the other three samples. Almost all the peaks matched quite well with those reported in the literature, confirming the formation of the pure anatase phase. The widening of Raman spectra at 144 cm^{-1} indicated the breakdown of long-range translational crystal symmetry, owing to the substitution of Ni ions into the TiO_2 lattice [53].

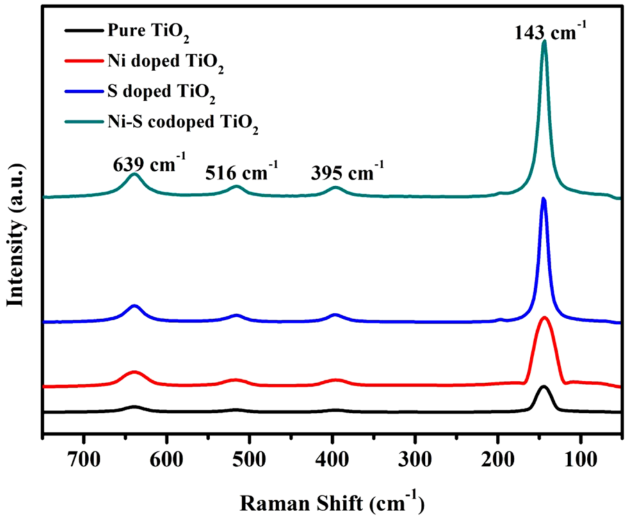

Fig. 6 Raman spectra for (a) pure TiO_2, Ni/TiO_2, S/TiO_2 and Ni-S/TiO_2 nanoparticles

The signature peak of TiO_2 in the codoped sample was significantly shifted, compared to that of the other TiO_2 sample, which may be ascribed to the reduction in crystallite sizes in the codoped TiO_2 [54]. The reduction in the size of the particles has also been confirmed by the help of SEM data. The obtained results from the Raman spectra were in perfect agreement with the literature reports [52].

3.6 UV- Visible Diffuse reflectance spectroscopy (DRS)

UV- Visible Diffuse reflectance spectroscopy was used to analyze the optical absorption properties of as-prepared samples and results were shown in Fig. 7a. The best light absorption of-S/TiO_2sample was examined compared with pure, Ni, and S/TiO_2 samples. It was specified as an improvement in the photocatalytic activity which occurs due to the presence of the Ni-Sinto the TiO_2 crystal structure. The bandgap energy of prepared samples was calculated using the Taucplot [55] and their results were shown in Fig. 7b. The bandgap of pure, Ni, Sand Ni-S /TiO_2NPs was obtained to be 3.04, 3.00, 2.93, and 2.87 eV respectively. The Ni-S /TiO_2shows a better red shift compared with Pure, Ni, and S doped TiO_2. This redshift of E_g could be interpreted as generally due to sp-d exchange interactions between the band electrons and the localized d electrons of the Ni^{2+} ion substituting S^{2-}lattice. The codoped sample is suggesting that Ni-S/TiO_2 NPs should possess the best visible light photocatalysis for the degradation of organic pollutants [56].

3.7 Flat band potential test

The role of doping and co-doping on the flat-band potential of TiO_2 nanostructures were investigated using Mott-Schottky (MS) plots under 1 kHz and shown in Fig. 8. All the TiO_2 samples presented n-type semiconductor property according to a positive slope in the MS plots. The obtained flat-band (V_{fb}) potential of pure, Ni, Sand Ni-S/TiO_2 samples were − 0.591,-0.621,-0.651 and − 0.699 eV vs Ag/AgCl (at pH = 13), respectively. The flat band potential of Ni-S/TiO_2 shifted more negative compare to that of the pure TiO_2. This negative shift indicated a larger accumulation of electrons in Ni-S/$TiO_2$and reflected decreased charge recombination [57]. More negative V_{fb} implied more favorable charge separation and transport efficiency when used as a

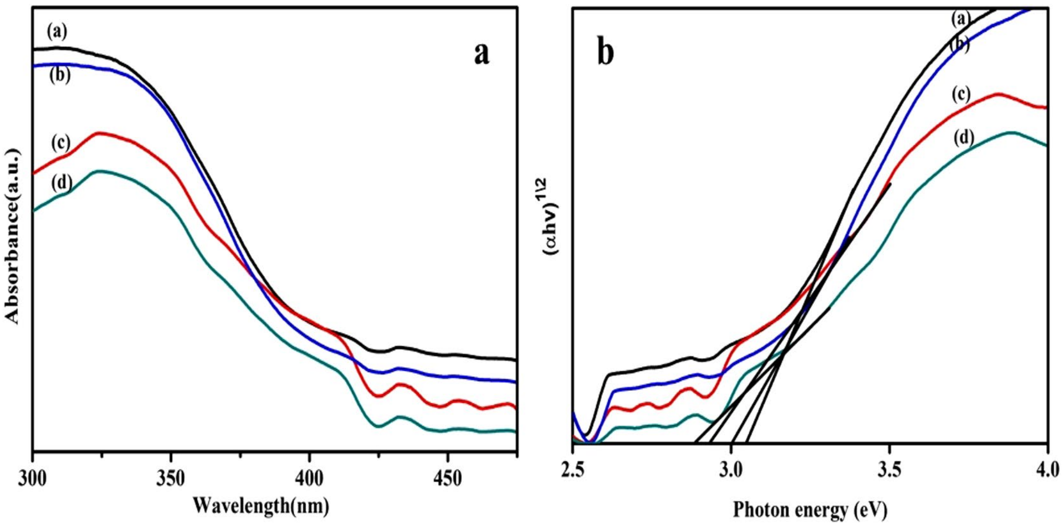

Fig. 7 (**a**) UV-diffuse reflectance spectra of (a) pure TiO_2, (b) Ni/TiO_2, (c) S/TiO_2, (d) Ni-S/TiO_2 and (**b**) plot of band gap energy of (a) pure TiO_2, (b) Ni/TiO_2, (c) S/TiO_2, (d) Ni-S/TiO_2 nanoparticles

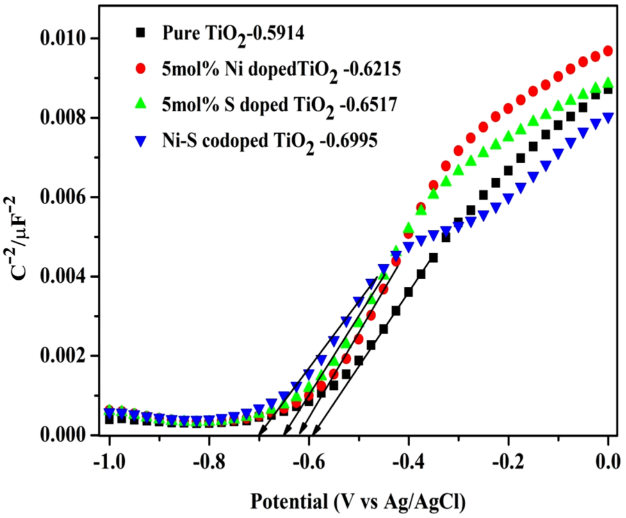

Fig. 8 Mott-Schottky plots of pure TiO_2, Ni/TiO_2, S/TiO_2, and Ni-S/TiO_2 nanoparticles

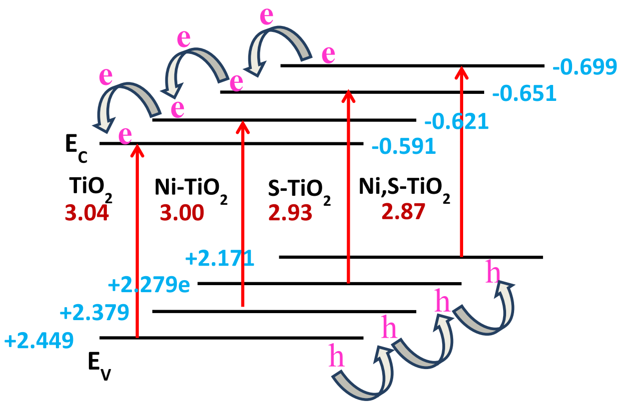

Fig. 9 Band structure of pure TiO_2, Ni/TiO_2, S/TiO_2 and Ni-S/TiO_2 nanoparticles

photocatalyst. The V_{fb} of n-type semiconductors were close to the CB potential (E_{CB}) [58]. Therefore, the E_{CB} values of the pure, Ni, S, and Ni-S/TiO_2 were – 0.591,-0.621,-0.651, and – 0.699 eV and the value of the E_{VB} can be calculated by the following equation:

$$E_{CB} = E_{VB} – E_g$$

The E_{VB} potentials of pure, Ni, Sand Ni-S/TiO_2were estimated as 2.449, 2.379, 2.279, 2.171 eV respectively [59, 60].

The E_{VB} values all the samples were around +2.449, + 2.379, + 2.279, + 2.171 eV respectively. At once, the decreases in the bandgap and shifting of the band edge to more negative values upon Ni-S/TiO_2 are not surprising. Because this effect occurs, the orbitals forming valence and conduction bands of Ni-S co-doping. The valence and conduction band of $TiO_2$is formed by O 2p and Ti 3d electrons. For the Ni-S/TiO_2 (Fig. 9), the E_{VB} maximum and E_{CB} minimum showed a negative shift after the introduction of Ti^{3+} states to the pure, Ni, S, and Ni-S/TiO_2. This was caused by lattice distortion and orbitals hybridization of 3d states with 2p states in the co-doping system [61, 62].

3.8 Photocatalytic activity

The photocatalytic performance of as-prepared samples was examined by the degradation of methylene blue (MB) under visiblelight irradiation. The dye degradation of the kinetic curve was obtained by plotting the (C/C_0) ratio as a function of irradiation time where C_0 and C designate the initial and residual concentrations of MB aqueous dye visible light irradiation. As shown in Fig. 10, the degradation of MB was negligible in a blank experiment. After added to the catalysis, clearly the pure TiO_2 sample showed aslight change for the degradation under visible light illumination, which was mainly due to the photosensitization of MB dye. The Ni-TiO_2 and S-TiO_2 samples demonstrated their ability to remove organic pollutants. Ni-S codoped sample had taken better photo activity activity compared to Ni/TiO_2 and S/TiO_2 samples. This fact could be reasoned that the band structure of TiO_2 has been affected by codoping. The photocatalytic activities of prepared samples were determined by monitoring the degradation of MB under the visible light irradiation (200-800 nm). The absorption intensity of MB at 660 nm was used to monitor the concentration of MB during the degradation process and the reaction absorption intensity was examined every 30 min. Figure 11, shown that the absorption spectra of Ni-S/TiO_2sample.Here, the

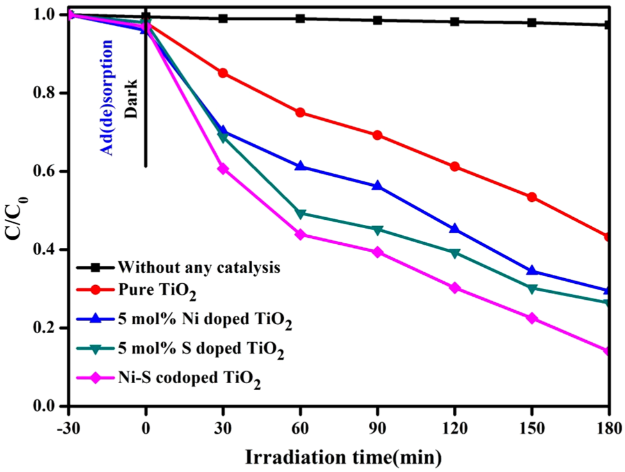

Fig. 10 Photocatalytic degradation of methylene blue in the presence of (a) Blank (b) Pure TiO_2 (c) Ni/TiO_2 (d) S/TiO_2 (e) Ni-S/TiO_2 under visible light irradiation

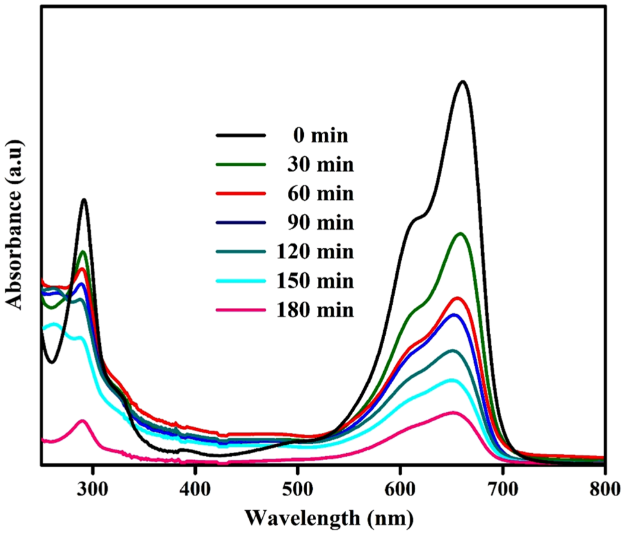

Fig. 11 The absorption spectrum of Ni-S/TiO_2 against MB under visible light irradiation

absorption peak intensity slowly decreased with the increase in irradiation time and disappeared after 180 min. Hence, the degradation percentage of Ni-S/TiO_2sample against MB was achieved by 85%. Therefore, the degradation efficiency of the present work is significantly compared with previously reported works in literature (Table 1).

3.9 Mechanism of degradation

The proposed mechanism of Ni-S/TiO_2 photocatalytic activity has been shown in Fig. 12. When the light illuminated on TiO_2 nanoparticles, the impinging photons possessing equal or higher energies than the bandgap energy of TiO_2 would excite the electrons from valence band(VB) to conduction band(CB), which resulted in the generation of excited electrons in the CB and positive holes in the VB. These electron-hole pairs are transferred inside the semiconductor particle. One part of them recombined, while others reached the surface and interacted with O_2, OH^- and H_2O, hence it's a resulted in the formation of reactive species [71, 72]. Transfer of trapped electron to oxygen molecule will produce $^{\bullet}O_2$ radical, while the trapped hole could interact with hydroxyl anion with the formation of $^{\bullet}OH$ radicals. The photocatalytic decompositions were inorganic molecules and ions, such as CO_2, H_2O, SO_4^{2-}. On this basis, we could determine the advantages of heterogeneous catalysis as a mean of purifying water from organic contaminants at room temperature without the use of chemical reagents and expensive physical-chemical systems [73].

3.10 Trapping experiments

To investigate the main reactive species responsible for the degradation of organic pollutants over Ni-S codoped TiO_2 NPs. The nanoparticles were carried out through trapping experiments in the presence of different sacrificial agents such as BQ, IPA, EDTA, and $AgNO_3$ utilized as the scavengers of $O^{\cdot}{}_2^{-}$, $OH^{\cdot}$, h^+ and e^- respectively [74]. As shown in Fig. 13, when $AgNO_3$ or IPA was added to the photocatalytic oxidation of the MB reaction system, the conversion of MB slightly decreased; when $AgNO_3$ or BQ was added the conversion of MB quickly abated. These results indicated that h^+ and $O^{\cdot}{}_2^{-}$ have a significant influence on the photocatalytic reaction, whereas the effect of the $OH^{\cdot}$ radical was negligible [75].

3.11 Reusability of Ni-S codoped TiO_2 nanoparticles

In practical applications nowadays, photocatalytic efficiency and stability both were significant features to extend the quality of the catalysts. The recycling experiment verified the stability and reusability of the Ni-S codoped TiO_2 nanoparticle and the results presented in Fig. 14. The MB dye

Table 1 Comparison of photocatalytic activity of different materials along with their degradation percentage and time

S.No	Material	Catalyst/Dye concentration	Dye	Degradation Percent(%)	Degradation Time (min)	References
1.	$Zr_2Ni_1Cu_7/Si_3N_4$TNAC	0.02 g/20 ppm	Methylene blue	92	90 min	[63]
2.	PANI/ZS	0.1 g/1.5 × 10^{-5} M	Methylene blue	82	120 min	[64]
3.	Cu supported on ZnO	0.15 g/45 ppm	Methylene blue	100	30 min	[65]
4.	GA-clpoly(AAm)/$Ni(OH)_2$/FeOOH NCH	0.2 g/100 ppm	Methylene blue	75	120 min	[66]
5.	Au-TiO_2@m-CN	0.2 g/100 ppm	Methylene Orange	90.4%	90 min	[67]
6.	TiO_2/WO_3	0.01 g/4 × 10^{-5} M	Methylene Orange	99.6%	250 min	[68]
7.	TiO_2 bycathodic arc deposition (CD1100 Flim)	2.5 cm × 2.5 cm/ 10 ppm	Cr(VI)	100%	300 min	[69]
8.	Pt@Fe-WO_3	0.4 g/40 ppm	ethylene	99.4%	240 min	[70]
10.	Ni/S codoped TiO_2	0.5 g/30 ppm	Methylene blue	85	180 min	Present study

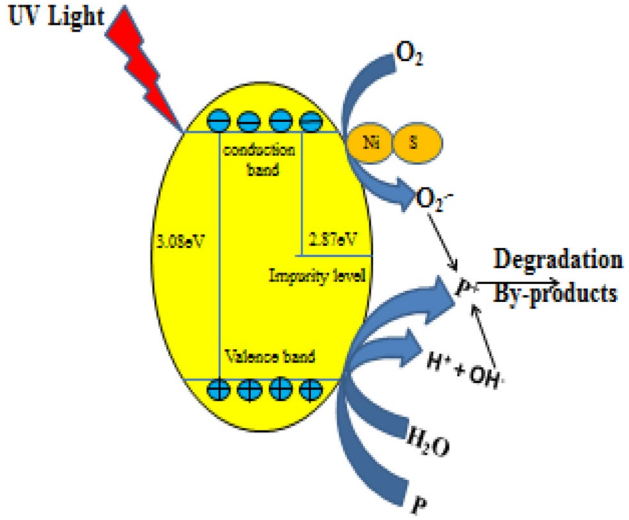

Fig. 12 Schematic description of the methylene blue photocatalytic mechanism of Ni-S/TiO_2 nanoparticles

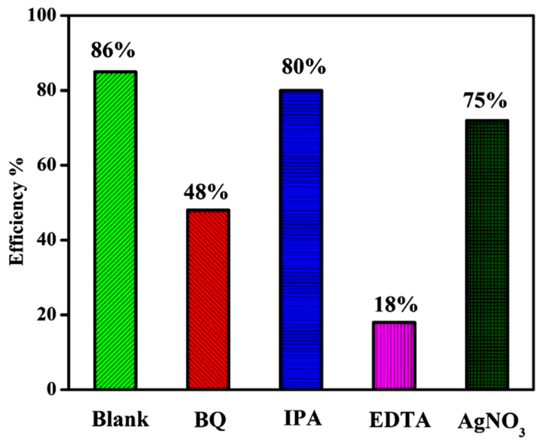

Fig. 13 Effect of BQ, IPA, EDTA, and $AgNO_3$ on MB degradation by Ni-S/TiO_2 NPs

was degenerated in every recycle with a similar degradation efficiency these effects demonstrating that there was no observable loss of photocatalytic activity after 4 cycles.

4 Conclusions

In this work, we designated pure, Ni-doped, S-doped, and Ni-S codoped TiO_2 nanoparticles that were efficiently prepared by the sol-gel method. The XRD from well-known that particles were anatase phase, the occurrence of hydroxyl ions, and Ti-O-Ti were confirmed using the FT-IR spectrum. The SEM images demonstrated the reduced particle size for codoped TiO_2 compared with pure and doped particles. The morphology variation was observed from promptly agglomerate to uniformly distribute in the spherical particle. The EDAX analysis confirmed the presence of doping ions. The bandgap energy was diminished from 3.08 eV to 2.87 eV for pure to codoped TiO_2 nanoparticles, indicating that interchange interaction occurred among the localized electrons and the band electrons in codoped TiO_2. Ni-S/TiO_2 was found to be an excellent photocatalytic activity for the degradation of MB under visible light irradiation. We describe an integrated effect between Ni-S/TiO_2 that significantly enhances the visible light photocatalytic performance for the degradation of MB under the visible light irradiation. Furthermore, Ni-S/TiO_2 NPs could be reused for 4 cycles without any obvious loss in their reactivity under visible light irradiation.

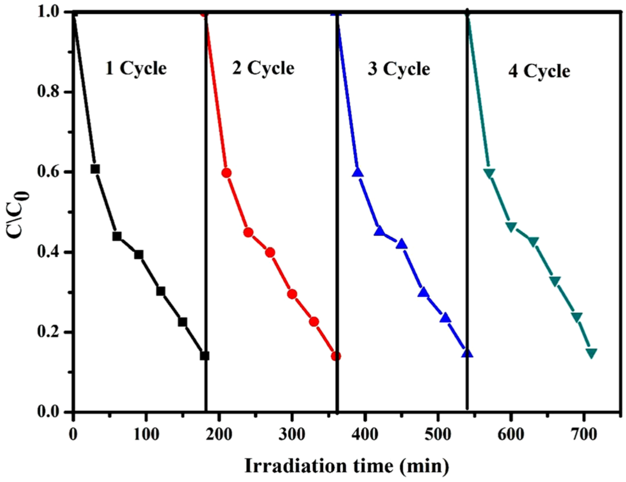

Fig. 14 Recycling experiments of Ni-S/TiO_2 nanoparticles

Compliance with ethical standards

Conflict of interest The authors should state "The author(s) declare(s) that there is no conflict of interest regarding the publication of this article." Submitting authors are responsible for coauthors declaring their interests.

References

1. G. Sharma, D. Pathania, M. Naushad, Preparation, characterization, and ion exchange behavior of nanocomposite polyaniline zirconium (IV) selenotungstophosphate for the separation of toxic metal ions. Ionics **21**(4), 1045–1055 (2015)
2. D. Barathi, N. Rajalakshmi, R. Ranjith, R. Sangeetha, S. Meyvel, Controllable synthesis of CeO_2/g-C_3N_4 hybrid catalysts and its structural, optical and visible light photocatalytic activity. Diam Relat Mater **108161** (2020)
3. Z. Mirzaeifard, Z. Shariatinia, M. Jourshabani, S.M. Rezaei Darvishi, ZnO photocatalyst revisited: Effective photocatalytic degradation of emerging contaminants using S-doped ZnO nanoparticles under visible light radiation. Ind. Eng. Chem. Res. **59**, 15894–15911 (2020)
4. R. Jaiswal, J. Bharambe, N. Patel, A. Dashora, D.C. Kothari, A. Miotello, Copper and Nitrogen co-doped TiO2 photocatalyst with enhanced optical absorption and catalytic activity. Appl. Catal. B-Environ. **168**, 333–341 (2015)
5. R. Ranjith, V. Krishnakumar, S. Boobas, J. Venkatesan, J. Ayaprakash, An efficient photocatalytic and antibacterial performance of Ni/Ce–Codoped CdS nanostructure under visible light irradiation. Chem. Select **3**, 9259–9267 (2018)
6. V.D. Dao, N.T.P. Le Chi, D. Van Thuan, T.D. Pham, D.T. Tran, M.P. Nguyen, P. Thao, M.V. Nguyen, N.T.D. Cam, N.M. Tuong, N.M. Dang, Superior stability and photocatalytic activity of Ta3N5 sensitized/protected by conducting polymers for water splitting. J. Alloys Compd. **775**, 942–949 (2019)
7. R. Rajendran, V. Jayaraman, K. Varadharajan, Fabrication of CdS/$PbWO_4$ nanocomposite to improve the photocatalytic degradation efficiency of methylene blue under visible light irradiation. J. Phys. Chem. Solids **129**, 261–269 (2019)
8. N. Duraisamy, K. Kandiah, R. Rajendran, S. Prabhu, R. Ramesh, G. Dhanaraj, Electrochemical and photocatalytic investigation of nickel oxide for energy storage and waste water treatment. Res. Chem. Intermed. **44**, 5653–5667 (2018)
9. R. Dumitru, A. Ianculescu, C. Pacurariu, L. Lupa, A. Pop, B. Vasile, A. Surdu, F. Manea, $BiFeO_3$-synthesis, characterization and its photocatalytic activity towards doxorubicin degradation from water. Ceram. Int. **45**, 2789–2802 (2019)
10. K. Chhor, Comparative studies of phenol and salicylic acid photocatalytic degradation influence of adsorbed oxygen. Mater. Chem. Phys. **86**, 123–131 (2004)
11. G. Colón, M.C. Hidalgo, J.A. Navío, Photocatalytic behavior of sulphated TiO_2 for phenol degradation. Appl. Catal. B Environ. **45**, 39–50 (2003)
12. E. Bandala, Solar photoreactors comparison based on oxalic acid photocatalytic degradation. Sol. Energy **77**, 503–512 (2004)
13. T. McMurray, Intrinsic kinetics of photocatalytic oxidation of formic and oxalic acid on immobilised TiO_2 films. Appl. Catal. A Gen. **262**, 105–110 (2004)
14. J.J. Murcia, M.C. Hidalgo, J.A. Navío, J. Araña, J.M. Doña-Rodríguez, Correlation study between photo-degradation and surface adsorption properties of phenol and methyl orange on TiO_2 vs platinum-supported TiO_2. Appl. Catal. B Environ. **150-151**, 107–115 (2014)
15. M.M.B. Abbad, A.A.H. Kadum, A.B. Mohamad, M.S. Takriff, K. Sopian, Synthesis and catalytic activity of TiO_2 nanoparticles for photochemical oxidation of concentrated chlorophenols under direct solar radiation. Int. J. Electrochem. Sci. **7**, 4871–4888 (2012)
16. S. Wang, J.S. Lian, W.T. Zheng, Q. Jiang, Photocatalytic property of Fe doped anatase and rutile TiO_2 nanocrystal particles prepared by sol-gel technique. Appl. Surf. Sci. **263**, 260–265 (2012)
17. B. Tain, C. Li, J. Zhang, One step preparation, characterization and visible-light photocatalytic activity of Cr-doped TiO_2 with anatase and rutile bicrystalline phase. Chem. Eng. J. **191**, 402–409 (2012)
18. A. Zaleska, Doped-TiO_2 a review. Recent Pat Eng. **2**, 157–164 (2008)
19. S. Ghasemi, S. Rahimnejad, S.R. Setayesh, S. Rohani, M.R. Gholami, Transition metal ions effect on the properties and photocatalytic activity of nanocrystalline TiO_2 prepared in an ionic liquid. J. Hazard. Mater. **172**, 1573–1578 (2009)
20. R. Asashi, T. Morikawa, T. Ohwaki, K. Aoki, Y. Taga, Visible-light photocatalysis in nitrogen-doped titanium oxides. Science **293**, 269–271 (2001)
21. H. Irie, Y. Watanabe, K. Hashimoto, Nitrogen-concentration dependence on photocatalytic activity of TiO_2-xNx powders. J. Phys. Chem. B **107**, 5483–5486 (2003)
22. C. Burda, Y.B. Lou, X.B. Chen, A.C. Samia, J. Stout, J.L. Gole, Enhanced nitrogen doping in TiO_2 nanoparticles. Nano Lett. **3**, 1049–1051 (2003)
23. S. Sakthivel, H. Kisch, Photocatalytic and photoelectrochemical properties of nitrogen-doped titanium dioxide. Chem. Phys. Chem. **4**, 487–490 (2003)
24. W. Ren, Z. Ai, F. Jia, L. Zhang, X. Fan, Z. Zou, Low-temperature preparation and visible light photocatalytic activity of mesoporous carbon-doped crystalline TiO_2. Appl. Catal. B Environ. **69**, 138–144 (2007)
25. Y. Choi, Y. Umebayshi, M. Yoshikawa, Fabrication and characterization of C-doped anatase TiO_2 photocatalysts. J. Mater. Sci. **3**, 1837–1839 (2004)
26. X. Tang, D. Li, Sulfur-doped highly ordered TiO_2 nanotubular arrays with visible light response. J. Phys. Chem. C **112**, 5405–5409 (2008)
27. F. Wei, L. Ni, P. Cui, Preparation and characterization of sulfur-doped TiO_2/Ti photoelectrodes and their photoelectrocatalytic performance. J. Hazard. Mater. **156**, 135–140 (2008)
28. J. Wang, S. Chen, Q. Li, J. Yang, Anatase TiO_2 codoping with sulfur and acceptor IIB metals for water splitting. Int. J. Hydrog. Energy **41**, 13050–13057 (2016)
29. G. Liu, X. Wang, Z. Chen, H.M. Cheng, G.Q. Lu, Supercritical preparation of a highly active S-doped TiO_2 photocatalyst for methylene blue mineralization. Environ. Sci. Technol. **41**, 4410–4414 (2007)
30. R. Long, N.J. English, Electronic properties of anatase-TiO_2 codoped by cationpairs from hybrid density functional theory calculations. Chem. Phys. Lett. **513**, 218–223 (2011)
31. X.G. Ma, Y. Wu, Y.H. Lu, J. Xu, Y.J. Wang, Y.F. Zhu, Effect of compensated codoping on the photoelectrochemical properties of anatase TiO_2 photocatalyst. J. Phys. Chem. C **115**, 16963–16969 (2011)
32. A. Biswas, A. Chakraborty, N.R. Jana, Nitrogen and fluorine codoped, colloidal TiO_2 nanoparticle tunable doping, large red-shifted band edge, visible light induced photocatalysis, and cell death. ACS Appl. Mater. Interfaces **10**, 1976–1986 (2018)
33. J.Z. Bloh, A. Folli, D.E. Macphee, Adjusting nitrogen doping level in titanium dioxide by codoping with tungsten properties and band structure of the resulting materials. J. Phys. Chem. C **118**, 21281–21292 (2014)
34. B. Parveen, M. Hassan, Z. Khalida, S. Riaz, S. Naseem, Original roomtemperature ferromagnetism in Ni-doped TiO_2 diluted magnetic semiconductor thin films. J Appl. Res. Technol. **15**, 132–13921292 (2017)
35. M.R. Elahifard, S. Ahmadvand, A. Mirzanejad, Effects of Ni-doping on the photo-catalytic activity of TiO_2 anatase and rutile: Simulation and experiment. Mater. Sci. Semicond. Process. **84**, 10–1621292 (2018)

36. S. Liu, X. Chen, A visible light response TiO_2 photocatalyst realized by cationic S-doping and its application for phenol degradation. J. Hazard. Mater. **152**, 48–55 (2008)
37. M.J. Uddin, M.A. Islam, S.A. Haque, S. Hasan, M.S.A. Amin, M.M. Rahman, Preparation of nanostructured TiO_2 based photocatalysts by controlling the calcining temperature and pH. Int Nanolett **2**, 1–10 (2012)
38. U.G. Akpan, B.H. Hameed, The advancements in sol-gel method of doped TiO_2 photocatalysts. Appl. Catal. A Gen. **375**, 1–11 (2010)
39. K. Varadharajan, B. Singaram, R. Mani, J. Jeyaram, Enhanced visible light photocatalytic activity of Ag and Zn doped and Codoped TiO_2 nanoparticles. J. Clust. Sci. **27**, 1815–1829 (2016)
40. C.L. Tang, X. Wei, Y.M. Jiang, X.Y. Wu, L.N. Han, K.X. Wang, J.S. Chen, Cobalt-doped MnO_2 hierarchical yolk-shell spheres with improved supercapacitive performance. J. Phys. Chem. C **119**, 8465–8471 (2015)
41. D.A.H. Hanaor, C.C. Sorrell, Review of anatase to rutile transformation. J. Mater. Sci. **46**, 855–874 (2011)
42. L.G. Devi, B.N. Murthy, S.G. Kumar, Photocatalytic activity of TiO_2 doped with Zn_2 and V_5 transition metal ions: Influence of crystallite size and dopant electronic configuration on photocatalytic activity. Mater. Sci. Eng. B **166**, 1–6 (2010)
43. P. Vijayan, C. Mahendiran, C. Suresh, K. Shanthi, Photocatalytic activity of iron doped nanocrystalline titania for the oxidative degradation of 2,4,6-trichlorophenol. Catal. Today **141**, 220–224 (2009)
44. M.V. Reddy, R. Jose, T.H. Teng, B.V.R. Chowdari, S. Ramakrishna, Preparation and electrochemical studies of electrospun TiO_2 nanofibers and molton salt method nanoparticles. Electrochim. Acta **55**, 3109–3117 (2010)
45. T.T. Loan, N.N. Long, Optical properties of anatase and rutile TiO_2 Cr_3 powders. VNU J Sci Math Phys. **30**, 59–67 (2014)
46. L. Kumaresan, A. Prabhu, M. Palanichamy, E. Arumugam, V. Murugesan, Synthesis and characterization of Zr_4, La_3 and Ce_3 doped mesoporous TiO_2 evaluation of their photocatalytic activity. J. Hazard. Mater. **186**, 1183–1192 (2011)
47. J. Yang, H. Bai, X. Tan, J. Lian, IR and XPS investigation of visible-light photocatalysis: Nitrogen-carbon-doped TiO_2 film. Appl. Surf. Sci. **253**, 1988–1994 (2006)
48. Y.C. Zhang, M. Yang, G. Zhang, D.D. Dionysiou, HNO_3-involved one-step low temperature solvothermal synthesis of N-doped TiO_2 nanocrystals for efficient photocatalytic reduction of Cr(VI) in water. Appl. Catal. B Environ. **142-143**, 249–258 (2013)
49. F. Dong, S. Guo, H. Wang, X. Li, Z. Wu, Enhancement of the visible light photocatalytic activity of c-doped TiO_2 nanomaterials prepared by a green synthetic approach. J. Phys. Chem. C. **115**, 13285–13292 (2011)
50. N. Venkatachalam, M. Palanichamy, V. Murugesan, Sol-gel preparation and characterization of alkaline earth metal doped nano TiO_2 efficient degradation of 4-chlorophenol. J. Mol. Catal. A Chem. **273**, 177–185 (2007)
51. I. Ganesh, A.K. Gupta, P.P. Kumar, P.S.C. Sekhar, K. Radha, G. Padmanabham, G. Sundararajan, Preparation and characterization of Ni-doped TiO_2 materials for photocurrent and photocatalytic applications. Sci. World J. **2012**, 1–16 (2012)
52. X. Chen, S.S. Mao, Titanium dioxide nanomaterials. Synthesis, properties, modifications, and applications. Chem Rev. **107**, 2891–2959 (2007)
53. M. Pal, U. Pal, J.M.G.Y. Jimenez, F. Perez-Rodriguez, Effects of crystallization and dopant concentration on the emission behavior of TiO_2. Eu nanophosphors. Nanoscale Res. Lett. **7**, 1–12 (2012)
54. D.B. Hamal, K.J. Klabunde, Synthesis, characterization and visible light activity of new nanoparticle photocatalysts based on silver, carbon and sulphur doped TiO_2. J. Colloid Interface Sci. **311**, 514–522 (2007)
55. V. Krishnakumar, R. Ranjith, J. Jayaprakash, S. Boobas, J. Venkatesan, Enhancement of photocatalytic degradation of methylene blue under visible light using transparent Mg-doped CdS–PVA nanocomposite films. J. Mater. Sci. Mater. Electron. **28**(18), 13990–13999 (2017)
56. T. Wang, J. Lang, Y. Zhao, Y. Su, Y. Zhao, X. Wang, Simultaneous doping and heterojunction of silver on Na_2 Ta_2O_6 nanoparticles for visible light driven photocatalysis: The relationship between tunable optical absorption, defect chemistry and photocatalytic activity. Cryst Eng Comm **17**(35), 6651–6660 (2015)
57. M. Ismael, Highly effective ruthenium-doped TiO_2 nanoparticles photocatalyst for visible-light-drivenphotocatalytic hydrogen production. New J. Chem. **43**, 9596 (2019)
58. R. Tao, S. Yang, C. Shao, X. Li, S. Liu, Y. Liu, Reusable and flexible g-C_3N_4/Ag_3PO_4/Polyacrylonitrile heterojunction nanofibers for photocatalytic dye degradation and oxygen evolution. ACS Appl. Nano Mat. **5**, 3081–3090 (2019)
59. N.M. Mohamed, R. Bashiri, F.K. Chong, S. Sufian, S. Kakooei, Photoelectrochemical behavior of bimetallic Cu-Niand monometallic Cu, Ni doped TiO_2 for hydrogenproduction. Int. J. Hydrogen Energy, 1–8 (2015)
60. A. Kumar, A. Rana, G. Sharma, M. Naushad, A.H. Al-Muhtaseb, C. Guo, A. Iglesias-Juez, F.J. Stadler, High-performance photocatalytic hydrogen production and degradation of levofloxacin by wide Spectrum-responsive Ag/Fe_3O_4 bridged $SrTiO_3$/g-C_3N_4 plasmonic nanojunctions: Joint effectof Ag and Fe_3O_4. ACS Appl. Mater. Interfaces **10**, 40474–40490 (2018)
61. P.S. Archana, E.N. Kumar, C. Vijila, S. Ramakrishna, M.M. Yusoff, R. Jose, Random nanowires of nickel doped TiO_2 with high surface area and electron mobility for highefficiency dye-sensitized solar cells. Dalton Trans. **42**(4), 1024–1032 (2013)
62. Z. Dong, D. Ding, T. Li, C. Ning, Facile preparation of Ti^{3+}/Ni co-doped TiO_2 nanotubes photoanode for efficient photoelectrochemical water splitting. Appl. Surf. Sci. **480**, 219–228 (2019)
63. G. Sharma, A. Kumar, S. Sharma, M. Naushad, T. Ahamad, S.I. Al-Saeedi, G.M. Al-Senani, N.S. Al-kadhi, F.J. Stadler, Facile fabrication of $Zr_2Ni_1Cu_7$ trimetallic nano-alloy and its compositewith Si_3N_4 for visible light assisted photodegradation of methylene blue. J. Mol. Liq. **272**, 170–179 (2018)
64. D. Pathania, G. Sharma, A. Kumar, N.C. Kothiyal, Fabrication of nanocomposite polyaniline zirconium(IV) silicophosphatefor photocatalytic and antimicrobial activity. J. Alloys Compd. **588**, 668–675 (2014)
65. A.G. Acedo-Mendoza, A. Infantes-Molina, D. Vargas-Hernandez, C.A. Chavez-Sanchez, E. Rodríguez-Castellon, J.C. Tanori-Cordova, Photodegradation of methylene blue and methyl orange with CuO supported on ZnO photocatalysts: The effect of copper loading and reaction temperature. Mater. Sci. Semicond. Process. **119**, 105257 (2020)
66. M. Naushad, G. Sharma, Z.A. Alothman, Photodegradation of toxic dye using Gum Arabic-crosslinked-poly(acrylamide)/$Ni(OH)_2$/FeOOH nanocomposites hydrogel. J. Clean. Prod. **241**, 118263 (2019)
67. R. Malik, V.K. Tomer, N. Joshi, T. Dankwort, L. Linand, L. Kienle, Au-TiO_2-loaded cubic g-C_3N_4 nanohybrids for photocatalytic and volatile organic amine sensing applications. ACS Appl. Mater. Interfaces **10**, 34087–34097 (2018)
68. V.O. Odhiambo, A. Ongarbayeva, O. Kéri, L. Simonand, I.M. Szilágyi, Synthesis of TiO_2/WO_3 composite nanofibers by a water-based electrospinning process and their application in photocatalysis. Nanomaterials **10**, 882 (2020)
69. A. Kleiman, J.M. Meichtry, D. Vega, M.I. Litter, A. Márquez, Photocatalytic activity of TiO_2 films prepared by cathodic arc

deposition: Dependence on thickness and reuse of the photocatalysts. Surface Coatings Technol., 125154 (2019)

70. X. Liu, H. Zhai, P. Wang, Q. Zhang, Z. Wang, Y. Liu, Y. Dai, B. Huang, X. Qinand, X. Zhang, Synthesis of a WO_3 photocatalyst with highphotocatalytic activity and stability usingsynergetic internal Fe^{3+}doping and superficial Ptloading for ethylene degradation under visible-light irradiation. Catalysis Sci. Technol. **3** (2019)
71. S. Boobas, V. Krishnakumar, J. Jayaprakash, R. Ranjith, J. Vijayan, Preparation of cerium and sulfurcodoped TiO_2 nanoparticles based photocatalytic activity with enhanced visible light. J. Photochem. Photobiol. A: Chem. **349**, 91–99 (2017)
72. Y. Nosaka, A.Y. Nosaka, Generation and detection of reactive oxygen species in photocatalysis. Chem. Rev. **117**, 11302–11336 (2017)
73. L.G. Devi, B.N. Murthy, S.G. Kumar, Photocatalytic activity of TiO_2 doped with Zn^{2+} and V^{5+} transition metal ions: Influence of crystallite size and dopant electronic configuration on photocatalytic activity. Mater. Sci. Eng. B-Adv. Funct. Solid-State Mater. **166**, 1–6 (2010)
74. X. Yang, H. Zhao, J. Feng, Y. Chen, S. Gao, R. Cao, Visible light-driven selective oxidation of alcohols using a dye-sensitized. J. Catal. **351**, 59–66 (2017)
75. W. Feng, G. Wu, L. Li, N. Guan, Solvent-free selective photocatalytic oxidation of benzyl alcohol over modified TiO_2. Green Chem. **13**, 3265–3272 (2011)